COO-1545-237
CONF-780826--3

Submitted

for the XIX International Conference

on High Energy Physics

Tokyo, 23-31 August 1978

Charge-Exchange Production of Axial Vector Mesons at 8.45 GeV/c*

K.W. Edwards and D. Legacey
Department of Physics, Carleton University, Ottawa, Ontario, Canada

P. Brockman, J. Gandsman, P.M. Patel, E. Shabazian and C. Zanfino
Department of Physics, McGill University, Montreal, Quebec, Canada

N.R. Stanton
Department of Physics, The Ohio State University, Columbus, Ohio, USA

J.A. Dankowych, J.F. Martin, A.J. Pawlicki, J.D. Prentice and T. S. Yoon
Department of Physics, University of Toronto, Toronto, Ontario, Canada

ABSTRACT

We present differential cross-sections for the reactions

$\pi^- p \to B^0(1235) n$, $B^0 \to \omega^0 \pi^0$ ($\omega^0 \to \pi^+ \pi^- \pi^0$), and $\pi^- p \to D^0(1285) n$, $D^0 \to \eta^0 \pi^+ \pi^-$ ($\eta^0 \to \gamma\gamma$)

at 8.45 GeV/c. The data were obtained at the Argonne ZGS with the Charged and Neutral Spectrometer which detected both charged pions and all γ rays in these final states.

*Work sponsored in part by DOE and NRC/IPP (Canada)

DISCLAIMER

Relatively little experimental information exists on charge exchange production of axial vector mesons. Such information is especially interesting because several members of the two axial vector nonets are either missing or poorly established. The A_1, for example, has not been unambiguously identified in forward charge exchange reactions, and the two isoscalar companions of the B, which can best be looked for in charge exchange production, have never been seen.

We present here differential cross section data for the reactions

(1) $\pi^- p \rightarrow D^o(1285)n$, $D^o \rightarrow \eta\pi^+\pi^-$, $\eta \rightarrow \gamma\gamma$

and

(2) $\pi^- p \rightarrow B^o(1235)n$, $B^o \rightarrow \omega^o\pi^o$, $\pi^o \rightarrow \gamma\gamma$, $\omega^o \rightarrow \pi^+\pi^-\pi^o$, $\pi^o \rightarrow \gamma\gamma$

at 8.45 GeV/c. The experiment was conducted at the Argonne ZGS with the Charged and Neutral Spectrometer, shown in Figure 1 and described in more detail elsewhere.[1,2] This apparatus measured the vector momenta of both charged pions and all γ's in the $\pi^+\pi^-\eta^o$ and $\omega^o\pi^o$ final states; the recoil neutron was not detected. Momentum analysis of the π^+ and π^- was performed in a large aperture magnetic spectrometer using conventional magnetostrictive spark chambers. Immediately downstream was a thin (1½ radiation length) lead converter followed by three magnetostrictive spark chambers to

record the shower conversion points. A rather coarse-grained array of 56 lead glass Cerenkov counters measured the shower energies. The whole apparatus was made as short and wide as possible to maximize the acceptance for these multiparticle final states: the magnet was less than a meter deep, and the 1.52 x 1.52 m^2 lead glass array was only 3.8 m from the hydrogen target. Scintillator hodoscopes allowed approximate selection of charged and shower multiplicities, and scintillator-lead sandwiches surrounding the target rejected most recoils other than neutrons.

The data sample presented here represents final analysis of 90% of the events collected before January, 1977. Our 1977 data, taken with a thicker converter, is currently being analyzed. It will eventually increase the statistics for reaction (1) by a factor of 2 to 3, and for reaction (2) by a factor of 3 to 5.

The Reaction $\pi^- p \to D^o n$.

Analysis of reaction (1) is summarized in Figures 2 and 3. Observing this reaction with $\eta \to \gamma\gamma$, rather than $\eta \to \pi^+\pi^-\pi^o$, has the distinct advantage of eliminating combinatorial backgrounds. Figure 2 shows spectra of $\gamma\gamma$ mass and nucleon mass squared for $\eta' \to \eta\pi^+\pi^-$ events, which are very clean, and for events above the η', which are somewhat dirtier. The arrows indicate the cuts on $M(\gamma\gamma)$ and $M^2(\text{nuc})$ for events to be retained. The η' peak resulting from a two constraint fit to events with the cuts is also shown.

The full $\eta\pi^+\pi^-$ mass spectrum from a 2C fit to the events surviving the cuts in Figure 2 is shown in Figure 3, both raw data (histogram) and with an approximate acceptance correction (points with error flags). The

histogram is dominated by the η' peak, scaled down by a factor of 10 to fit on the page. A second prominent narrow peak which we identify with the D meson is centered at a mass of 1276 MeV.

We have studied the sensitivity of the D mass to systematic errors in measured variables such as γ energy, and have concluded that it is very difficult to move the D peak more than $\pm$ 3 MeV without producing completely unacceptable masses for the η and/or η'. We thus quote $M_D = 1276 \pm 3$ Mev. The width of the D peak in Figure 3 is 25 to 35 MeV. A Monte Carlo simulation of our experimental resolution, which reproduces the widths of the η, η' and nucleon peaks, indicates that the meson mass resolution is 20 MeV FWHM at 1275 MeV. The natural width of the D therefore lies in the range 15 to 30 MeV.

Preliminary results from an isobar-model phase shift analysis of the data in Figure 3 have been submitted to this Conference.[3] These results strongly support the $J^P = 1^+$ assignment for the D.

To obtain the differential cross section the narrow D signal was extracted by making a background subtraction in each bin of momentum transfer t. The D region was taken as 1.25 - 1.30 GeV, and the intervals 1.175 - 1.225 and 1.325 - 1.375 were used for the background estimate. Signal and background were of comparable size in all bins of t. There is still a very significant D peak even beyond $-t = 0.80$.

Corrections were applied to the data for events cut from the tails of the D, η and neutron peaks (.75, .86 and .95 respectively), for trigger and chamber efficiency losses, γ conversion efficiency, and for unseen decay

modes of the η. A Monte Carlo acceptance appropriate to a 1+ object decaying via $\delta\pi$ was used.[3] We estimate that the systematic error in the data is approximately $\pm$ 20%.

The Reaction $\pi^- p \to B^o n$.

The procedure[4] used to extract the B^o differential cross section is illustrated in Figure 4. Reaction (2) has four gammas in the final state, so there are three possible combination of $\gamma\gamma$ pairs to make each π^o. We have kept only that combination of $\gamma\gamma$ pairs for each event with the highest probability for the 2C fit to the $2\pi^o$ hypothesis. The spectrum of masses for this best combination is plotted in Figure 4a. Each event contributes two $\gamma\gamma$ pairs to the histogram. Events for which the χ^2 probability for the 2C fit is greater than 5%, and for which both π^o masses lie between 95 and 175 MeV, were retained for further analysis.

The histogram of nucleon missing mass for events with the 2C fit is shown in Figure 4b. Events with nucleon mass between 0.55 and 1.2 GeV and with χ^2 probability greater than 5% for the 3C fit to the $\pi^+\pi^-\pi^o\pi^o n$ final state were kept. The $\pi^+\pi^-\pi^o$ mass (two combinations per event) for these 3C-fit events is histogrammed in Figure 4c. There is a prominent ω peak with a measured width of 26 MeV, dominated by the experimental resolution. Events with at least one combination of $\pi^+\pi^-\pi^o$ mass in the interval .74 - .82 GeV were subjected to a 4C fit which assumed zero natural width for the ω. Once again, only events with confidence level greater than 5% were retained.

For approximately half of these events there remained an ambiguity of which π^o to assign to the ω. This decision was made on the basis of the Dalitz plot density for ω decay, which is known to be nearly linear in the variable $\lambda = |\vec{p}_+ \times \vec{p}_-|^2$. For the ambiguous events the combination with the higher value of λ was chosen. Figure 4d illustrates this procedure: the unshaded histogram is of all acceptance-corrected combinations from the ω region (0.75 - 0.82 GeV) of Figure 4c, while the shaded histogram corresponds to the selected combination.

The final sample of 1782 $\omega^o\pi^o$ events is shown in Figure 4e; it is dominated by the B^o peak. A good fit to this spectrum is obtained from a linear combination of acceptance-corrected $\omega^o\pi^o$ phase space, a Breit-Wigner shape for the B^o, and a small amount of distorted $B^o\Delta^o$ background. The resulting parameters for the B^o are $M(B^o) = 1232 \pm 8$ MeV, $\Gamma(B^o) = 147 \pm 20$ MeV, in reasonable agreement with those[5] for the charged B. This fit was repeated, with fixed mass and width of the B^o in four bins of t to determine the fraction of B^o events in the mass region 1155 - 1305 MeV as a function of t; this fraction varied from 0.58 to 0.75. The background subtractions for the smaller t bins used for the differential cross-section were obtained by interpolating between these fitted points.

Corrections to the data were applied for events lost in the B tails and in the χ^2 probability cuts, for trigger losses and chamber inefficiency, γ conversion probability, geometric acceptance and unseen decay modes of the ω^o. We believe that the largest systematic errors arise from uncertainty in the conversion efficiency for 4γ, and from uncertainty in the acceptance because of the presently unknown distribution of B^o helicities, giving rise to a total estimated $\pm$ 30% systematic uncertainty in the

differential cross section.

Differential Cross Sections

The differential cross sections for $\pi^- p \to D^o n \hookrightarrow \eta\pi^+\pi^-$ and $\pi^- p \to B^o n \hookrightarrow \omega^o\pi^o$ are presented in Figure 5. To compare these data note that B decays predominantly[5] into $\omega\pi$, while $D^o \to \eta\pi^+\pi^-/\text{all}$[6] is about $\frac{2}{3}(0.5) = 0.3$. Also shown in Figure 5 is the differential cross section for the pseudoscalar charge exchange reaction $\pi^- p \to \eta' n$ from this experiment. The production of η' is believed to be dominated by A_2 exchange, which has also been proposed[7,8] as the most important mechanism in producing B^o and D^o.

The shape of the D^o cross section is quite flat, roughly described by e^{3t}, with no evidence for the forward turnover predicted[7] on the basis of A_2 exchange, which couples mainly to helicity flip at the baryon vertex. The B^o data, which have better statistics over a more limited t range, definitely have no forward turnover and are completely consistent in shape with the D^o data in the region of overlap in t. Results from the phase shift analysis[3] indicate that the D^o is produced mostly ($\sim$80%) with t-channel helicity zero.

The integrated B^o cross section is quite small, about 11 μb, significantly less than the small η' cross section which is suppressed by the strange quark content of the η'. After branching ratio corrections the D^o cross section is even smaller, about 5 μb.

It thus appears, both from the lack of forward turnover and from the small integrated cross sections, that A_2 exchange does not play a strong role in B^o and D^o production. A similar conclusion has been reached[9]

from analysis of charged B production. Exchange degeneracy arguments[8] then suggest that ρ exchange should not contribute strongly to the charge exchange production of the A_1 or of the isoscalar members of the B nonet.

REFERENCES

1. M.H. Shaevitz et al., Phys. Rev. Lett. 36, 5 (1976).
2. M.H. Shaevitz, Ph.D. Thesis, Ohio State University (1975).
3. K.W. Edwards et al., "Results from a Partial Wave Analysis of the $\eta\pi^+\pi^-$ System Produced in $\pi^- p \to \eta\pi^+\pi^-$ at 8.45 GeV/c", submitted to this Conference.
4. P. Brockman, M.S. Thesis, McGill University (in preparation).
5. Particle Data Group, Rev. Mod. Phys. 48, S1 (1976).
6. H. Grässler et al., Nucl. Phys. B121, 189 (1977).
7. G.C. Fox and A.J.C. Hey, Nucl. Phys. B56, 386 (1973).
8. A.C. Irving and V. Chaloupka, Nucl. Phys. B89, 345 (1975).
9. U. Karshon et al., Phys. Rev. D10, 3608 (1974).

FIGURE CAPTIONS

Figure 1. Plan view of the Charged and Neutral Spectrometer. The scale along the beam direction has been slightly expanded for clarity, and the spark chambers which measure the beam direction are not shown.

Figure 2. Effective mass of $\gamma\gamma$ and nucleon mass squared for the η' region (a,b) and for events above the η' (c,d); effective mass of $\eta\pi^+\pi^-$ in the η' region (e).

Figure 3. Effective mass of $\eta\pi^+\pi^-$.

Figure 4. (a) $\gamma\gamma$ mass spectrum from $\pi^-p \to \pi^+\pi^-(4\gamma)$ (missing mass) (two combinations per event).

(b) Missing mass spectrum from $\pi^-p \to \pi^+\pi^-\pi^o\pi^o$ (missing mass).

(c) $\pi^+\pi^-\pi^o$ spectrum from $\pi^-p \to \pi^+\pi^-\pi^o\pi^on$ (two combinations per event).

(d) Histogram of acceptance-corrected events vs. $\lambda = (\vec{p}_+ \times \vec{p}_-)$ for both assignments of π^o to the ω (unshaded), and for the chosen combination (shaded).

(e) $\omega^o\pi^o$ mass spectrum for the final data sample. The vertical lines indicate the region used to obtain the B^o differential cross section.

Figure 5. Differential cross sections for $\pi^-p \to B^on$, $B^o \to \omega^o\pi^o$; $\pi^-p \to D^on$, $D^o \to \eta\pi^+\pi^-$; $\pi^-p \to \eta'n$, $\eta' \to$ all.

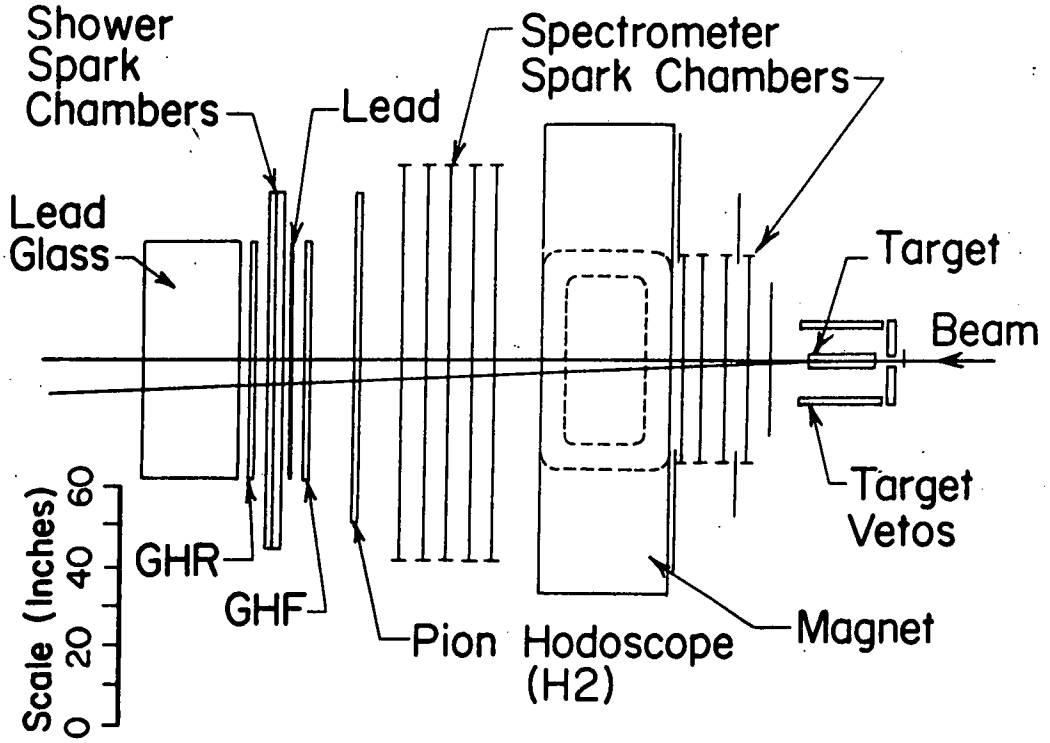
Shower
Spark
Chambers
Lead
Spectrometer
Spark Chambers
Lead
Glass
Target
Beam
Target
Vetos
GHR
GHF
Pion Hodoscope
(H2)
Magnet
Scale (Inches)
0
20
40
60

Figure 1

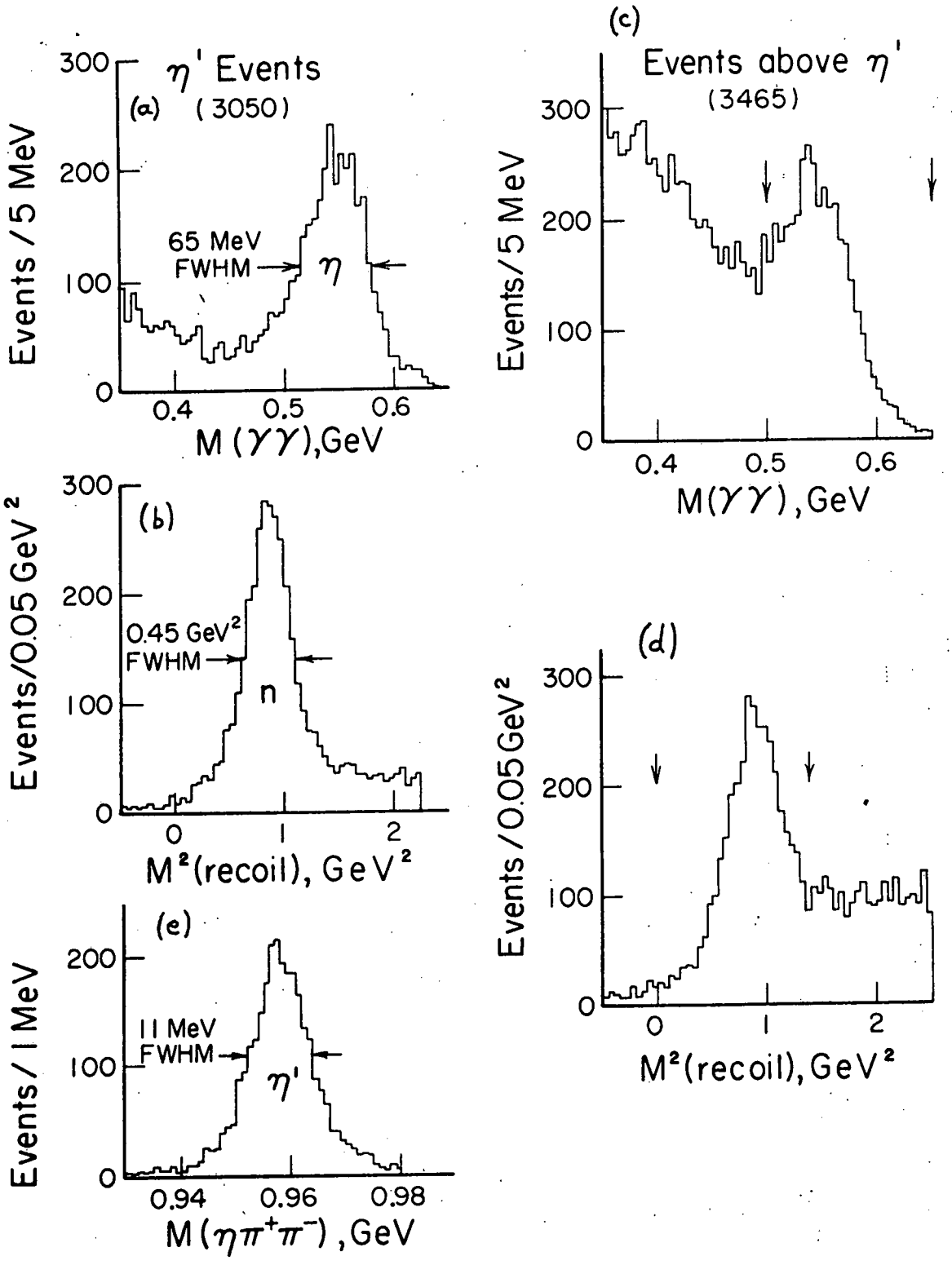
η' Events
(a) (3050)
65 MeV FWHM
η
Events / 5 MeV
M (γγ), GeV
(b)
0.45 GeV² FWHM
n
Events/0.05 GeV²
M²(recoil), GeV²
(e)
11 MeV FWHM
η'
Events / 1 MeV
M (ηπ⁺π⁻), GeV
(c)
Events above η'
(3465)
Events/5 MeV
M(γγ), GeV
(d)
Events /0.05 GeV²
M²(recoil), GeV²

Figure 2

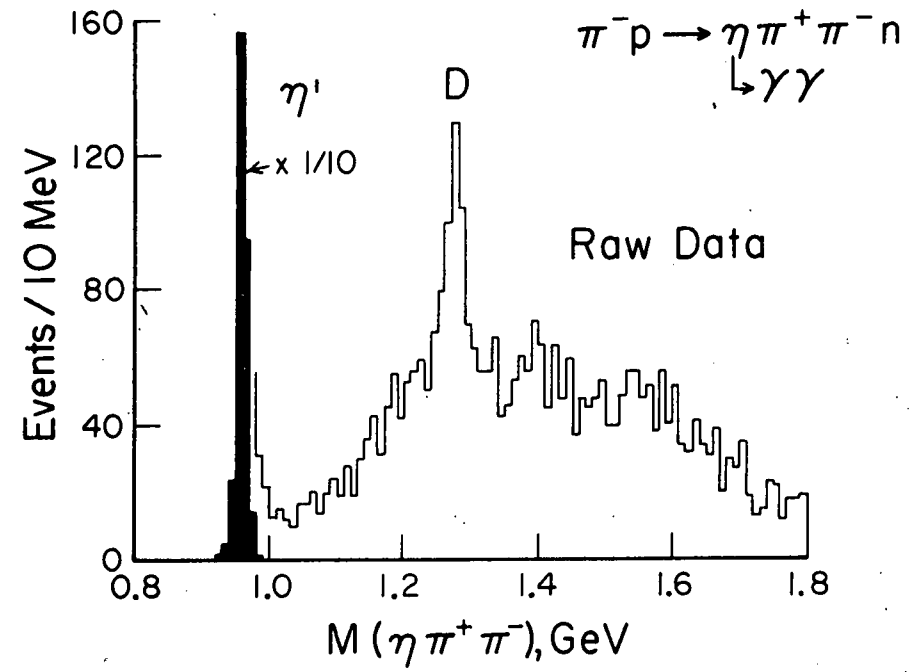
$\pi^- p \to \eta \pi^+ \pi^- n$
$\hookrightarrow \gamma\gamma$
η'
D
x 1/10
Raw Data
Events / 10 MeV
160
120
80
40
0
0.8
1.0
1.2
1.4
1.6
1.8
$M(\eta \pi^+ \pi^-)$, GeV

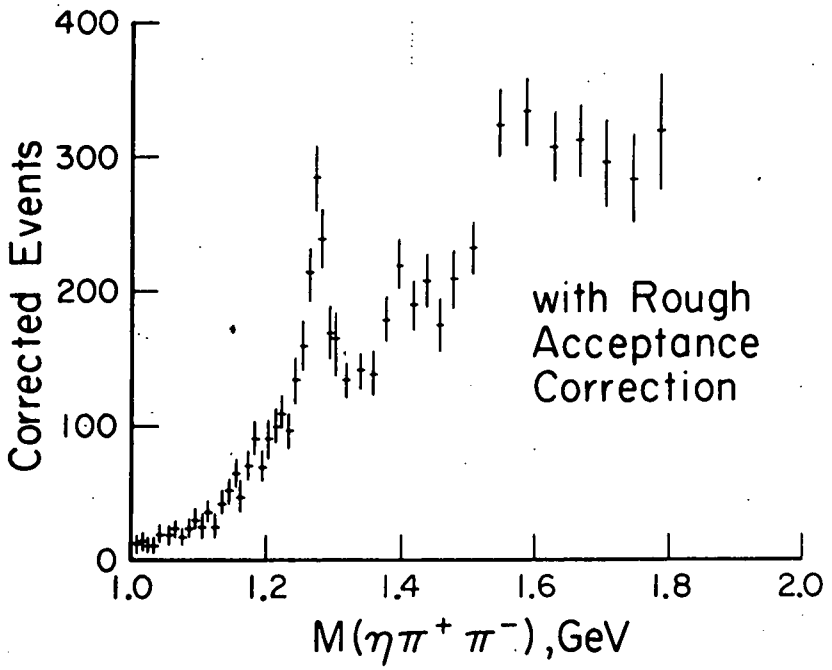
with Rough
Acceptance
Correction
Corrected Events
400
300
200
100
0
1.0
1.2
1.4
1.6
1.8
2.0
$M(\eta \pi^+ \pi^-)$, GeV

Figure 3

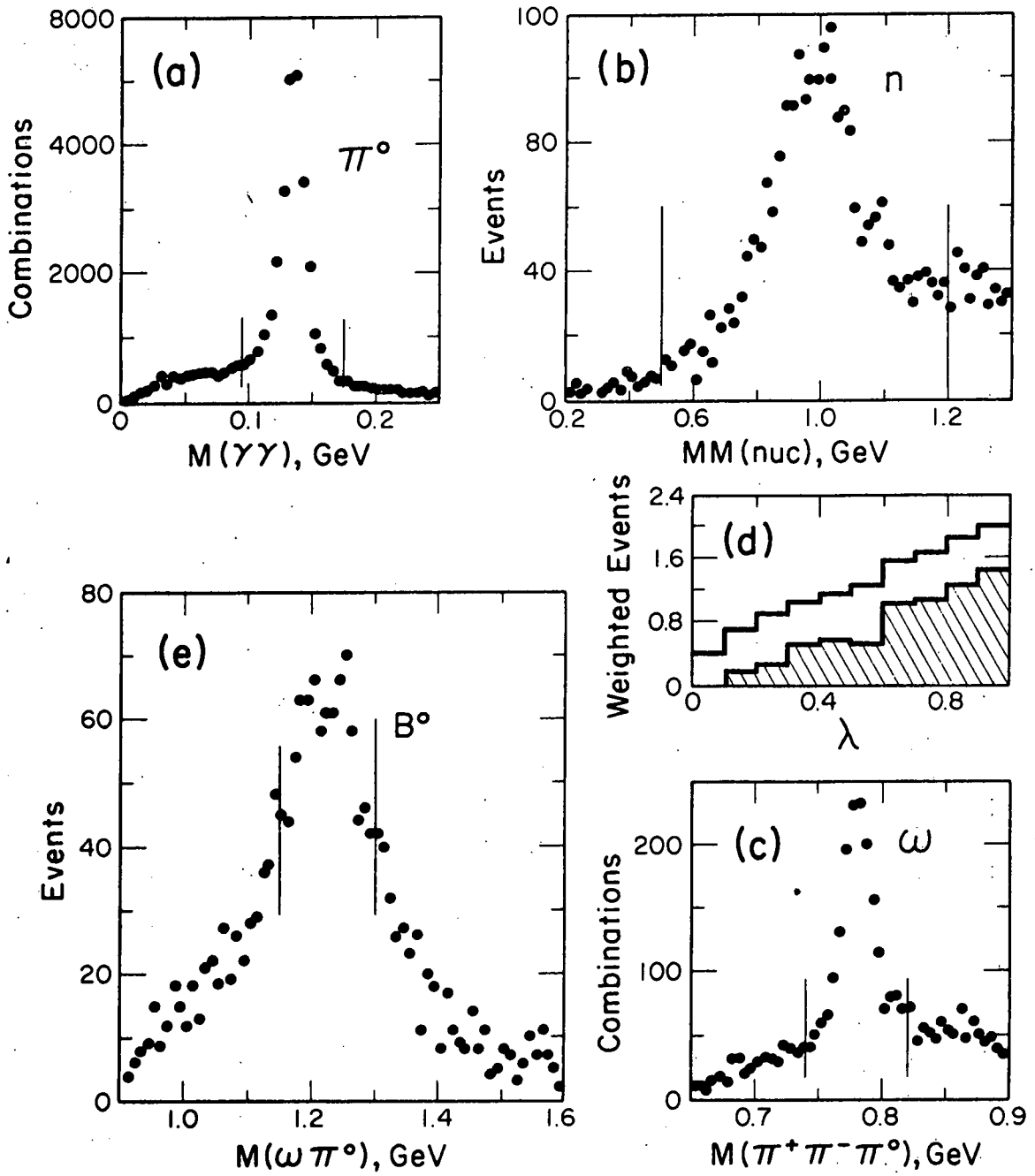
(a)
π°
Combinations
8000
4000
2000
0
0
0.1
0.2
M(γγ), GeV
(b)
n
Events
100
80
40
0
0.2
0.6
1.0
1.2
MM(nuc), GeV
(d)
Weighted Events
2.4
1.6
0.8
0
0
0.4
0.8
λ
(e)
B°
Events
80
60
40
20
0
1.0
1.2
1.4
1.6
M(ω π°), GeV
(c)
ω
Combinations
200
100
0
0.7
0.8
0.9
M(π⁺π⁻π°), GeV

Figure 4

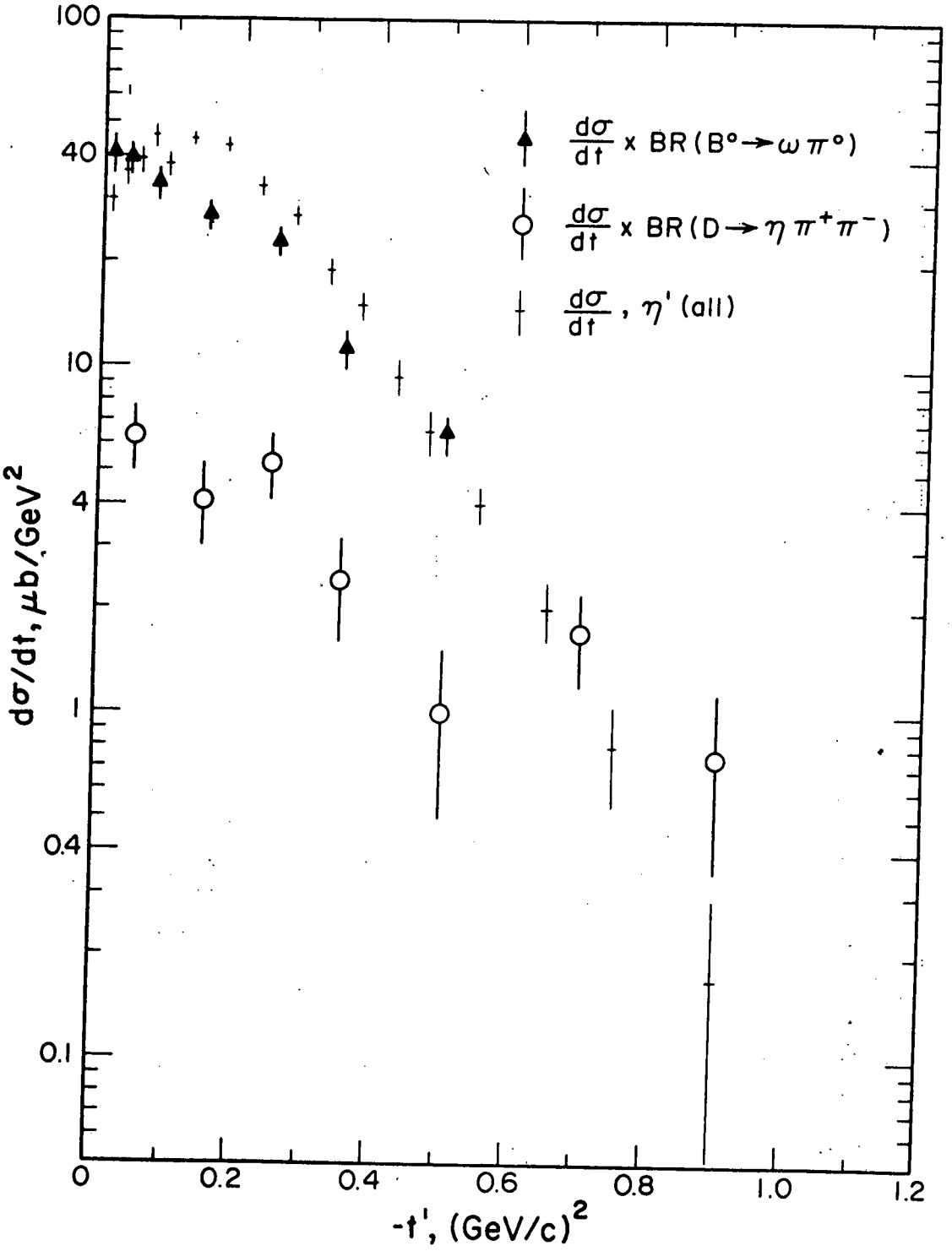
100
40
10
4
1
0.4
0.1
0
0.2
0.4
0.6
0.8
1.0
1.2
dσ/dt, μb/GeV²
-t', (GeV/c)²
dσ/dt x BR(B°→ωπ°)
dσ/dt x BR(D→ηπ⁺π⁻)
dσ/dt, η'(all)

Figure 5